Insights into noncanonical E1 enzyme activation from the structure of autophagic E1 Atg7 with Atg8

Seung Beom Hong[1], Byeong-Won Kim[1], Kyung-Eun Lee[2], Se Woong Kim[1], Hyesung Jeon[2], Joon Kim[1] & Hyun Kyu Song[1]

Autophagy is the degradation of cellular organelles via the lysosomal pathway. The autophagic ubiquitin-like (Ubl) molecule Atg8 is activated by the E1-like enzyme Atg7. As this noncanonical E1 enzyme's domain organization is unique among Ubl-activating E1 enzymes, the structural basis for its interactions with Atg8 and partner E2 enzymes remains obscure. Here we present the structure of the N-terminal domain of Atg7, revealing a unique protein fold and interactions with both autophagic E2 enzymes Atg3 and Atg10. The structure of the C-terminal domain of Atg7 in complex with Atg8 shows the mode of dimerization and mechanism of recognition of Atg8. Notably, the catalytic cysteine residue in Atg7 is positioned close to the C-terminal glycine of Atg8, its target for thioester formation, potentially eliminating the need for large conformational rearrangements characteristic of other E1s.

Autophagy, a bulk degradation process of a cell's own proteins by lysosomes (or vacuoles in fungi), is tightly regulated to maintain a balance between synthesis and degradation of cellular products[1,2] and is an important mechanism for recycling amino acids from cellular proteins under metabolically stressful conditions such as starvation[2]. Recently there have been several substantial advances in understanding of autophagy, including identification of the *atg* genes, linking of specific human diseases to autophagy, and biochemical and structural investigation of some Atg proteins[1,3–9]. Despite these results, many molecular details of autophagy remain unknown.

One noteworthy feature of autophagosome formation is analogous to ubiquitylation[1,10,11]. Many known Ubl modifiers are conjugated to their targets through sequential enzymatic reactions catalyzed by E1 activating enzymes, E2 conjugating enzymes and E3 ligase enzymes[12–14]. E1 enzymes are classified into two groups, canonical and noncanonical, depending on domain architectures and enzymatic mechanisms[15], and crystal structures of several canonical E1 enzymes such as SUMO, NEDD8 and ubiquitin E1s have revealed details of their reaction mechanisms[16–19]. In contrast, although the structure of one noncanonical E1 enzyme has been determined (Uba5)[20], there is relatively little structural and biochemical information about the diverse noncanonical E1 enzymes.

The essential autophagic enzyme Atg7 is a noncanonical E1 enzyme involved in many cellular processes, including autophagosome formation, amino acid supply, mitochondrial clearance, clearance of ubiquitin-positive aggregates, maintenance of hematopoietic stem cells and plant immunity toward fungal infection[21–25]. Atg7 has several unique features as compared with other E1 enzymes. It consists of a previously uncharacterized N-terminal domain and a C-terminal domain that contains a catalytic cysteine residue, an adenylation site and an oligomerization region[26] that mediates homodimerization. The E1-like Atg7 activates two distant homologs of ubiquitin, Atg8 and Atg12, in an ATP-dependent manner. These activated Ubl molecules are then transferred to the E2-like enzymes Atg3 and Atg10, respectively[4], before conjugation to other proteins via C-terminal glycine residues in a manner analogous to ubiquitylation[21,27].

Canonical E1 enzymes contain two adenylation domains, a catalytic cysteine domain and a ubiquitin-fold domain (UFD)[15]. Although Atg7 has an evolutionarily related adenylation domain, it lacks a separate catalytic cysteine domain. Instead, a catalytic Cys507 residue lies within the adenylation domain. Additionally, Atg7 lacks a UFD but contains a unique N-terminal domain with no clear sequence similarity to any component of the canonical ubiquitin pathway (**Fig. 1a**). In all canonical E1 enzymes that have been characterized, a UFD mediates interaction with the respective E2 enzyme[15]; the lack of a UFD in Atg7 raises the question of how this enzyme recognizes its cognate E2s, Atg3 and Atg10. Finally, the divergent domain architecture and oligomeric state of Atg7 are suggestive of differences in Ubl recognition, activation and transfer that remain to be explored.

Here we describe structural and biochemical characterization of *Saccharomyces cerevisiae* Atg7 and its interactions with Atg8, Atg3 and Atg10. The 2.1-Å-resolution crystal structure of the N-terminal domain of Atg7 (Atg7N) reveals a unique protein fold, and our biochemical data show that this domain binds both the autophagic E2s Atg3 and Atg10. The crystal structure of the C-terminal domain of Atg7 (Atg7C) in complex with Atg8 (Atg7C–Atg8), determined at 1.9-Å resolution, reveals the mechanisms of dimerization and recognition of Atg8 and shows that the adenylation site is preformed in

the absence of bound ATP. Notably, it also shows that the active site cysteine residue is closely juxtaposed with the C terminus of Atg8, its target for activation. Thus, unlike canonical E1s, Atg7 seems not to require a major conformational rearrangement in the course of Atg8 activation.

RESULTS

Overall structure of the Atg7C–Atg8 complex

The dimeric Atg7C (residues 293–630) shares clear sequence similarity with canonical E1 enzymes and is responsible for all functions related to E1 enzyme activity except for E2 enzyme binding (**Fig. 1a**). Indeed, we found that the isolated Atg7C fragment forms a covalent Atg7C~Atg8 conjugate in an ATP-dependent manner (**Fig. 1b**). E2 recognition is achieved by the unique Atg7N, as described below.

The crystal structure of Atg7C–Atg8 complex reveals a compact dimer with approximate dimensions of 85 Å × 72 Å × 50 Å (**Table 1** and **Fig. 1c**). Each subunit (residues Asp294–Glu620) consists of 11 α-helices, four 3_{10}-helices, and eight β-strands and connecting loops, and includes the adenylation region, a zinc-binding site and a catalytic cysteine residue (Cys507) for thioester bond formation. Comparison to other E1s of known structure using the DALI server[28] shows that homodimeric MoeB (PDB 1JWA) and ThiF (PDB 1ZFN) have the highest structural similarity (*Z* score > 25.0). The adenylation domains of canonical E1 enzymes such as ubiquitin-activating enzyme E1 (Uba1; PDB 3CMM), SUMO-activating enzyme (Uba2; PDB 1Y8Q) and NEDD8-activating enzyme (Uba3; PDB 3GZN) also show very high structural similarity (**Supplementary Fig. 1**). Structural similarity between Atg7C and the adenylation domain of canonical E1 enzymes was anticipated, given that they catalyze the same chemical reaction and that they share the highest sequence similarity in this region (**Supplementary Fig. 2a**). Notably, the mode of dimerization is similar among Atg7, MoeB and ThiF. The recent structure of ubiquitin-like modifier-activating enzyme 5 (PDB 3H8V), a minimalistic noncanonical E1 enzyme, also reveals a homodimeric state[20]. In contrast, canonical E1 enzymes either are monomeric or form heterodimers.

In addition to the core adenylation domain, Atg7C contains additional C-terminal helices (α14, α15, α16 and α17) that are located on the end of the domain far from the dimerization interface (**Fig. 1c**). The C-terminal helix α17, which was initially implicated in dimerization[26], is not involved in oligomerization. A mutant with this helix deleted has previously been reported to be dimeric as judged by cross-linking[29], and we find that it is dimeric in solution as well. Instead, this C-terminal region plays a crucial role in the binding with Atg8. The overall shape of $Atg7C_2–Atg8_2$ heterotetramer is similar to that of $MoeB_2–MoaD_2$ and $ThiF_2–ThiS_2$ complexes[30,31], and any dissimilarities stem mainly from the characteristic C-terminal helices (**Fig. 1c**). In canonical E1 structures the UFD follows the active adenylation domain, and it is noteworthy that in Atg7 the spatial orientation of the characteristic C-terminal region relative to the adenylation domain is similar to that of the UFD relative to the adenylation domain in a canonical E1 enzyme, although the Atg7 C-terminal region and the E1 UFD are structurally distinct[16,17,32].

A zinc atom is located between the adenylation domain and the C-terminal helical region. The zinc ion is tetrahedrally coordinated by four conserved cysteine residues (Cys485, Cys488, Cys569 and Cys572; **Fig. 2a**). The distances between zinc and ligand sulfur atoms (2.36 Å on average) are within the frequently observed range[33]. Similar zinc coordination is found in most other E1 structures[30–32]. The zinc-binding site is in close proximity to a loop connecting strand β3 and helix α3 of Atg8, and thus it is likely to be important for interaction with Atg8 (**Fig. 2a**).

The Atg7C dimer interface is formed largely by hydrophobic residues, with two polar interactions (**Supplementary Table 1**). These residues are very well conserved in Atg7 from different organisms (**Supplementary Fig. 2a**). The buried surface area upon dimerization is approximately 4,850 Å^2. The dimerization interface is elongated, with an eccentricity of 0.5 as calculated by the protein-protein interaction server PROTORP (http://www.bioinformatics.sussex.ac.uk/protorp/)[34].

Interaction between Atg7C and Atg8

The binding surface for Atg8 can be divided into two parts: one region for binding the core of the domain and another for recognition of its C-terminal tail, including Gly116, the target of adenylation. The C-terminal helices of Atg7, in particular α17, are crucial for coordination of the core of Atg8. The binding interface between Atg7C and Atg8 is formed primarily by hydrophobic residues, with some contribution from polar residues and hydrogen bonds (**Supplementary Fig. 2** and **Supplementary Table 2**). The buried surface area of the Atg7C–Atg8 complex is approximately 2,300 Å^2, comparable to complexes between E1 enzymes and Ubls (1,650 to 3,350 Å^2; refs. 16,17,32).
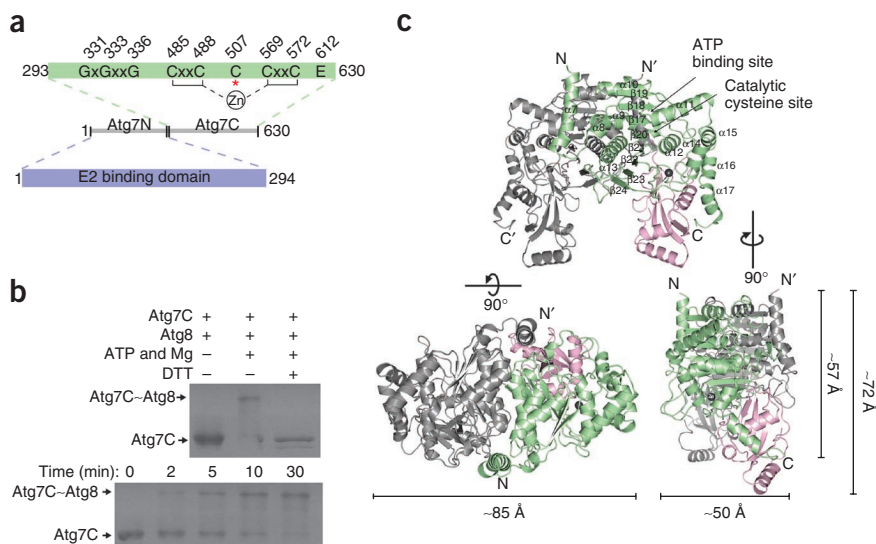
Figure 1 Structure of Atg7C–Atg8 complex and formation of Atg7C~Atg8 conjugate. (**a**) Domain architecture of Atg7 from *S. cerevisiae*. The N-terminal domain construct (Atg7N; residues 1–294) binds to autophagic E2 enzymes Atg3 and Atg10. The C-terminal domain (Atg7C; residues 293–630) contains an adenylation motif (GxGxxG), zinc binding region (two CxxC motifs) and catalytic Cys507 (red asterisk). (**b**) Top, formation of thioester Atg7C~Atg8 conjugate in the presence of ATP and magnesium ion. Bottom, time-dependent formation of Atg7C~Atg8 conjugates. (**c**) Ribbon diagram of the structure of the Atg7C–Atg8 complex showing 2:2 stoichiometry. In one Atg7C–Atg8 pair, Atg7C is colored green and Atg8 is pink; the other pair is colored gray. The secondary structural elements are sequentially labeled (from the Atg7N domain; see **Fig. 5a**). The N- and C-terminal residues of Atg7C are also labeled (prime symbol (′) denotes the second subunit; N, Asp293; C, Glu620).
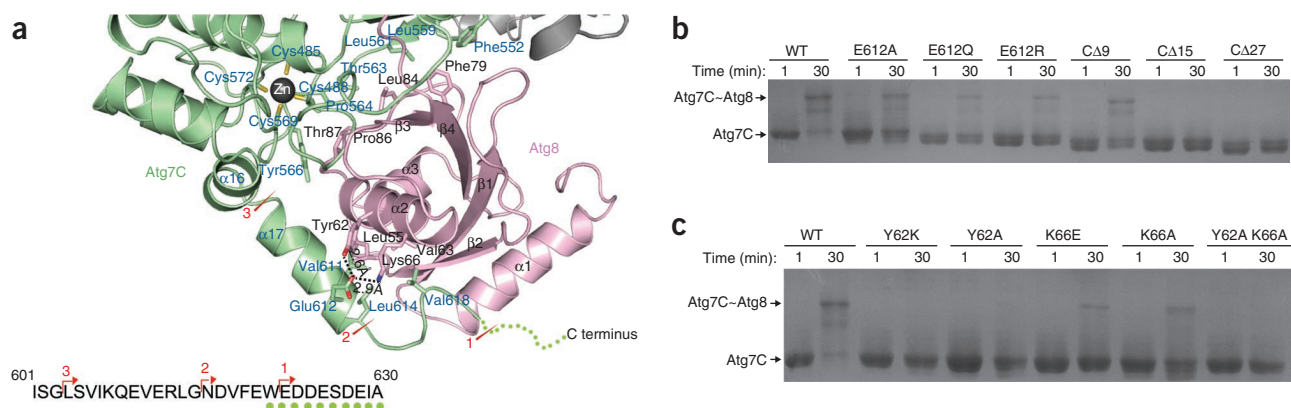
Figure 2 Atg8 recognition by the C-terminal region of Atg7C. (**a**) Detailed view of the interaction between the C-terminal region of Atg7C and Atg8. Three different deletion constructs representing 9-, 15- and 27-residue deletions from the C-terminus (Ala630) of Atg7C are marked as 1 (CΔ9), 2 (CΔ15) and 3 (CΔ27), respectively. The ten-residue C-terminal region of Atg7C absent in the electron density map is indicated as dots. The residues involved in the interaction are labeled in black and blue for Atg8 and Atg7C, respectively. Four cysteine residues (Cys485, Cys488, Cys569 and Cys572) coordinate a zinc atom (black) in tetrahedral geometry. (**b**) Effects of Atg7 mutations at the binding interface. WT, Atg7 wild type. (**c**) Effects of Atg8 mutations at the binding interface. WT, Atg8 wild type. See **Supplementary Figure 3b** for analysis of the mutations' effects in yeast.

As noted above, the C-terminal helices are crucial for Atg8 recognition and have been classified as a noncanonical E1-specific region[15]. The ten residues at the C terminus of Atg7C are not visible in the electron density map, suggesting that the last stretch is not involved in complex formation (**Fig. 2a**). For further analysis we generated three C-terminal deletion mutants of Atg7 (CΔ9, with a 9-residue deletion from the C-terminal end; CΔ15, 15-residue deletion; CΔ27, 27-residue deletion). The purified proteins were all dimers in solution. The CΔ9 mutant still catalyzes thioester bond formation, confirming that this invisible acidic stretch in our electron density map is not crucial for binding (**Fig. 2b**). The longer deletion mutants, CΔ15 and CΔ27, showed no thioester bond formation (**Fig. 2b**). These truncated mutants lack interacting residues, which explains the previous *in vivo* observation that an Atg7 CΔ17 mutant is defective in Atg8 lipidation for autophagosome formation[29].

The hydrophobic residues Val611, Leu614 and Val618 in the C-terminal stretch of Atg7 form a hydrophobic core with Leu55 and Val63 from Atg8 (**Fig. 2a**). In addition to the hydrophobic interactions, acidic Glu612 forms a hydrogen bond with Tyr62 and an ionic interaction with Lys66 in Atg8. To further dissect this interaction, we generated Atg7C mutants E612A, E612Q and E612R and assessed their thioester bond formation activity (**Fig. 2b**). All were impaired in their formation of the Atg7C~Atg8 conjugate, and much of Atg7C remained unmodified. However, some residual thioester bond formation activity was detected, most probably because the point mutations were not sufficient to disrupt the extensive hydrophobic interactions described above. We further investigated the importance of this interaction by performing the same activity assay after mutating Atg8 as follows: Y62K, Y62A, K66E, K66A, and Y62A K66A (**Fig. 2c**). Mutation of Lys66 resulted in a substantial reduction in Atg7C~Atg8 formation, and mutation of Tyr62 completely abolished conjugate formation. Consistent with this, mutant yeast strains expressing Y62K or Y62A K66A protein were defective in the formation of autophagosomes (**Supplementary Fig. 3a,b** and **Supplementary Methods**). Tyr62 of Atg8 is well conserved in many species but not in mammals (**Supplementary Fig. 2b**).

Adenylation and thioester bond formation sites
The Atg7C−Atg8 complex was crystallized in the absence of ATP. However, superposition of our Atg7C structure with the ATP-bound structure of Uba2 (ref. 32) reveals that most of the key residues that accommodate the ATP ligand are perfectly aligned in both structures (**Fig. 3a**). This indicates that the residues involved in the adenylation reaction are almost identical to those of the canonical E1 enzymes, and that the conformation of the adenylation domain in Atg7 can accommodate Atg8 without ATP ligand.

Perhaps the most notable feature of this Atg7C complex structure is the location of the catalytic cysteine residue (Cys507) and its proximity to the C-terminal glycine residue of Atg8, which is the target of adenylation and thioesterification. In contrast to canonical E1 enzymes, Atg7 has no isolated domain for thioester bond formation (the so-called 'active catalytic Cys domain'). Rather, the catalytic cysteine residue is located within the adenylation domain (**Fig. 1a**). Comparison of the Atg8 structure in the Atg7C−Atg8 complex with free Atg8 shows that no substantial conformational changes are induced in Atg8 upon complex formation (r.m.s. deviation of 108 matching Cα atoms is ~0.8 Å). The C-terminal tail of Atg8 is coordinated in the adenylation domain in an extended conformation and is stabilized by numerous hydrogen bonds and a salt bridge to its main chain (**Fig. 3b**, **Supplementary Fig. 4** and **Supplementary Table 2**). Notably, the distance between the carbonyl carbon atom of the C-terminal Gly116 residue of Atg8 and the sulfur atom of Cys507 (actually an oxygen atom in the present structure, as we crystallized the C507S mutant) is only 7.4 Å, which is much smaller than the distance observed in other E1 enzymes (~30 Å) as well as in the minimalistic noncanonical E1 Uba5 (16.8 Å)[16,17,20,32]. However, it is similar to the distance observed in the SUMO E1~SUMO1-AVSN tetrahedral intermediate analog[18]. This implies that no marked conformational change is required for formation of the covalent tetrahedral intermediate in Atg7. Additionally, the expected orientation of the nucleophilic sulfur atom in our structure differs from that seen in the SUMO E1~SUMO1-AVSN structure. Therefore, the present structure suggests that the thioesterification reaction may occur via a combination of a simple rotation of the side chain of Cys507 and a modest local conformational change of the 'crossover loop', the polypeptide segment immediately preceding the short helix containing Cys507 (**Fig. 3c**). The adenylation reaction is also absolutely necessary for thioester bond formation in Atg7, as it is in canonical E1 enzymes (**Fig. 1b**). However, the current structure, in which the adenylation and thioester bond formation sites are both in close proximity to the C terminus of Atg8, shows that a distinctly
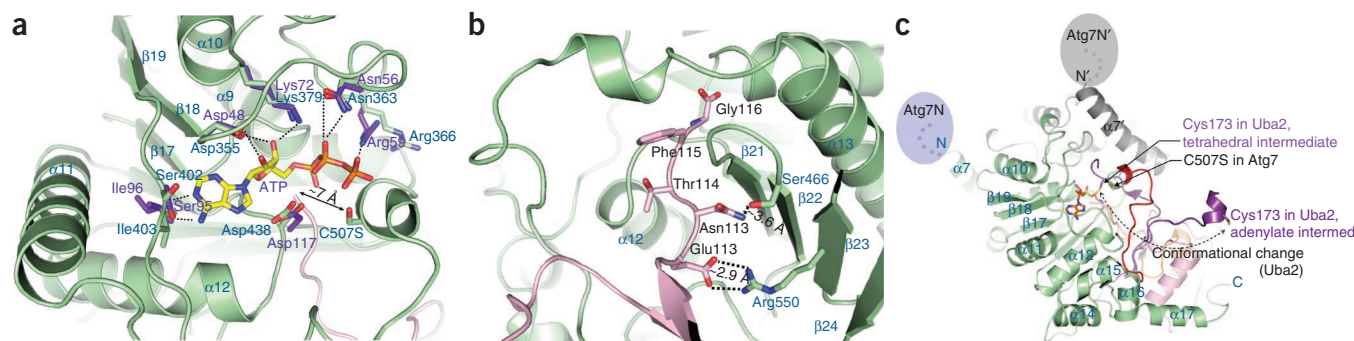
Figure 3 Active site of Atg7C–Atg8 complex. (**a**) Detailed view of the catalytically active region of Atg7C (green) and C-terminal segment of Atg8 (pink). The ATP-bound structure of Uba2, the SUMO E1 enzyme (PDB 1Y8Q; only the side chains of several residues and ATP are shown for clarity), is superposed with the Atg7C–Atg8 structure. (**b**) C-terminus of Atg8 extends into the binding site of Atg7. Several hydrogen bond and salt bridge interactions are illustrated. See **Supplementary Figure 4** and **Supplementary Table 2** for more details. (**c**) Comparison between the crossover loop region of Atg7C and that of Uba2 in two different conformations. The crossover loops in canonical E1 enzyme Uba2 and noncanonical Atg7 are colored purple and red, respectively. Note that the first helix, α7′, and the subsequent E2-binding region Atg7N′ (gray) from a different subunit are closer to the active site of Atg7C than are the equivalent regions from the same polypeptide chain (helix α7 and Atg7N, blue), which are located at the back side of the molecule.

different and much more modest conformational rearrangement accompanies catalysis in this noncanonical E1.
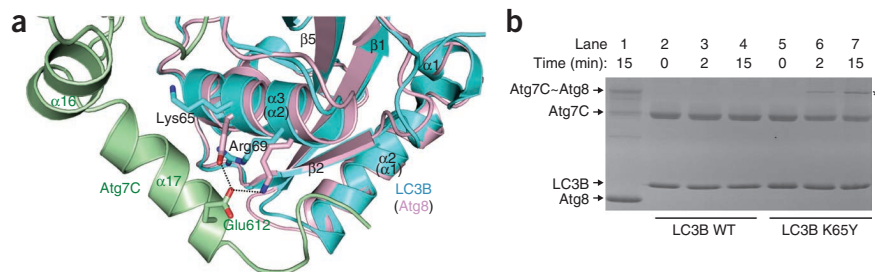
Interaction between LC3B mutant K65Y and Atg7C

Atg8 and its human homolog LC3B (also called MAP1LC3B, microtubule-associated protein 1 light chain 3β) share a high degree of sequence and structural similarity (sequence identity of 35.3% and r.m.s. deviation of 1.0 Å for 108 superimposed Cα atoms in Atg8 and LC3B; **Supplementary Fig. 2b** and **Fig. 4a**). However, specificity among species clearly exists. Yeast Atg7C is unable to catalyze the thioester bond formation with human LC3B (**Fig. 4b**, lanes 2–4). Notably, key interacting residues Tyr62 and Lys66 in Atg8 are replaced with Lys65 and Arg69 in the sequence of mammalian LC3B (**Supplementary Fig. 2b**). We further investigated the importance of those residues by swapping them between the yeast and human sequences. We generated LC3B mutants K65Y and R69K and examined their binding affinity to yeast Atg7 using gel filtration. Wild-type LC3B and the R69K mutant were unable to bind Atg7, whereas the K65Y mutant coeluted with Atg7 in solution (data not shown). Furthermore, under the same reaction conditions in which wild-type LC3B did not form a thioester bond with Atg7C, the K65Y mutant was conjugated to Atg7 (**Fig. 4b**). Consistent with this, the Atg8-deleted yeast strain expressing LC3B was defective in the formation of autophagosomes, but the strain expressing K65Y mutant recovered this activity (**Supplementary Fig. 3c**). It is noteworthy

that a single mutation of LC3B (K65Y) is sufficient to impart binding and generation of a thioester conjugate with yeast Atg7 and, consequently, to restore autophagosome formation in Atg8-null yeast.
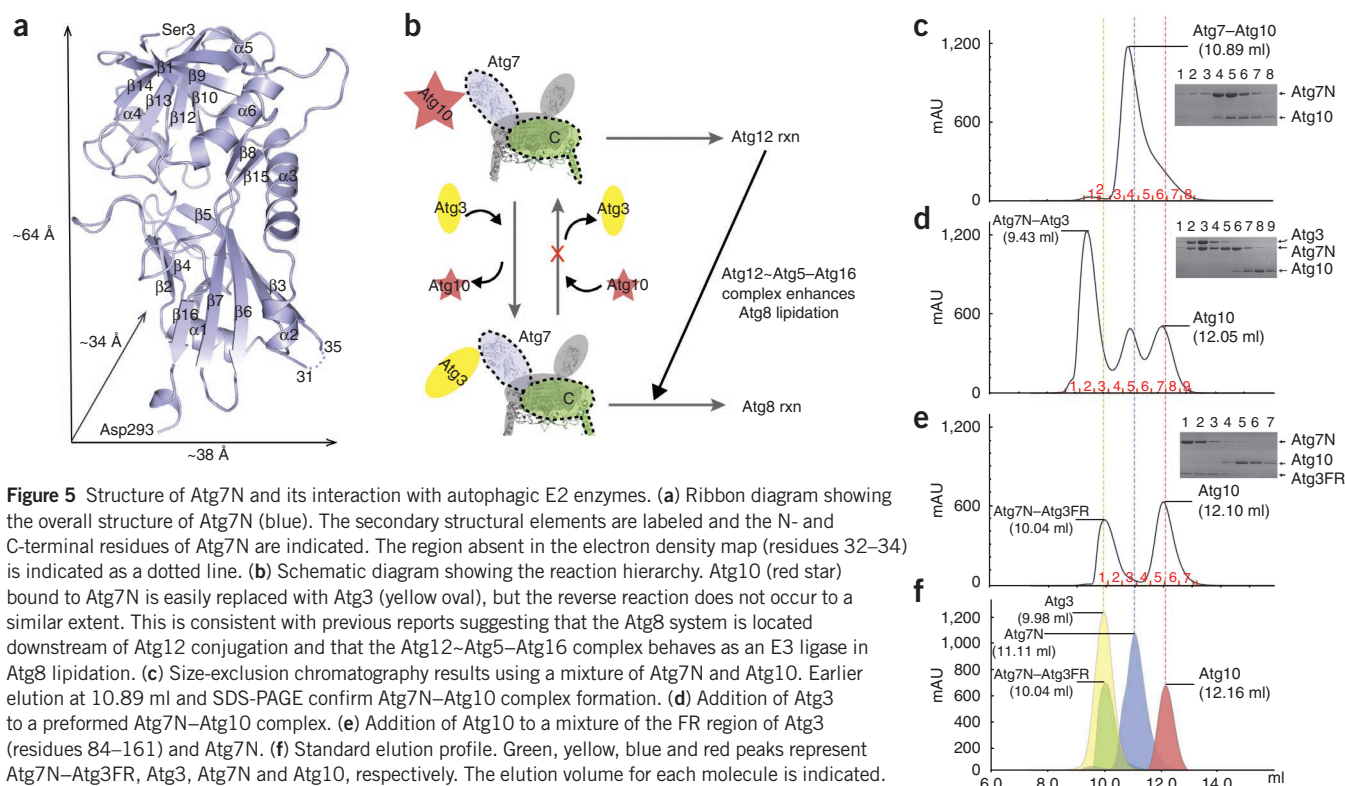
Structure of Atg7N

The isolated Atg7N (residues 1–294) is monomeric and has an elongated shape with approximate dimensions of $64 \times 38 \times 34$ Å (**Fig. 5**). It consists of six α-helices, three 3_{10}-helices, 16 β-strands and connecting loops organized in two structural subdomains (the upper and lower domains as depicted in **Fig. 5a**). Although Atg7N lacks detectable primary sequence homology with other proteins, we found substantial structural similarity with MPN family proteins, some of which are known to bind ubiquitin or Ubl proteins[35,36]. The Z scores as determined by the DALI server for Atg7N were 4.7, 4.5, 3.9, 3.3 and 3.2 for 26S proteasome non-ATPase regulatory subunit 7 (PDB 2O95), pre-mRNA splicing factor prp8 (PDB 2P87), JAMM from *Archaeoglobus fulgidus* (PDB 1R5X), the Mov34/MPN/Pad-1 family (PDB 2KCQ) and AMSH-like protease (PDB 2ZNR), respectively. These MPN-family proteins superimpose on Atg7N with an r.m.s. deviation in the range of ~3.0–4.0 Å for ~90–110 matching Cα atoms. Only the first (upper) subdomain of Atg7N shares structural homology with the aforementioned proteins. Because the Atg7N shows partial structural homology with ubiquitin binding proteins, we wondered whether there might be a direct interaction between Atg7N and Atg8.

However, we did not detect complex formation by gel filtration (**Supplementary Fig. 5a**) or in a pulldown assay (data not shown). We then examined the binding of Atg7N to ubiquitin. As with Atg8, we did not detect an interaction by gel filtration (**Supplementary Fig. 5b**) or in a pulldown assay (data not shown). We then examined complex formation between Atg7N and E2 enzymes Atg3 and Atg10. Both Atg7N–Atg3 and Atg7N–Atg10 formed a 1:1 complex in solution (**Fig. 5c,d** and **Supplementary Fig. 6a**). Although the exact binding region(s) in Atg7N for E2 enzymes remain to be determined, it is clear that Atg7N can interact with both Atg3 and Atg10. Therefore, we defined Atg7N as an 'autophagic E2-binding domain' (**Fig. 1a**).

Figure 4 Interaction between yeast Atg7 and human LC3B mutant. (**a**) Structural superposition of human LC3B with Atg8. Atg7C and Atg8 are colored as in **Figure 1c**, and LC3B is colored blue, with secondary structure elements labeled. The helix equivalent to α3 in LC3B is α2 in Atg8, as indicated in parentheses. (**b**) Effect of K65Y mutation of human LC3B. Lane 1, control showing position of the thioester Atg7C~Atg8 conjugate. Other lanes show a time-dependent conjugation reaction using a mixture of yeast Atg7C and human LC3B wild-type (WT) or K65Y mutant. Asterisk marks the thioester conjugate Atg7C~LC3B. See **Supplementary Figure 3c** for the effect of mutations in yeast.

Figure 5 Structure of Atg7N and its interaction with autophagic E2 enzymes. (**a**) Ribbon diagram showing the overall structure of Atg7N (blue). The secondary structural elements are labeled and the N- and C-terminal residues of Atg7N are indicated. The region absent in the electron density map (residues 32–34) is indicated as a dotted line. (**b**) Schematic diagram showing the reaction hierarchy. Atg10 (red star) bound to Atg7N is easily replaced with Atg3 (yellow oval), but the reverse reaction does not occur to a similar extent. This is consistent with previous reports suggesting that the Atg8 system is located downstream of Atg12 conjugation and that the Atg12~Atg5–Atg16 complex behaves as an E3 ligase in Atg8 lipidation. (**c**) Size-exclusion chromatography results using a mixture of Atg7N and Atg10. Earlier elution at 10.89 ml and SDS-PAGE confirm Atg7N–Atg10 complex formation. (**d**) Addition of Atg3 to a preformed Atg7N–Atg10 complex. (**e**) Addition of Atg10 to a mixture of the FR region of Atg3 (residues 84–161) and Atg7N. (**f**) Standard elution profile. Green, yellow, blue and red peaks represent Atg7N–Atg3FR, Atg3, Atg7N and Atg10, respectively. The elution volume for each molecule is indicated.

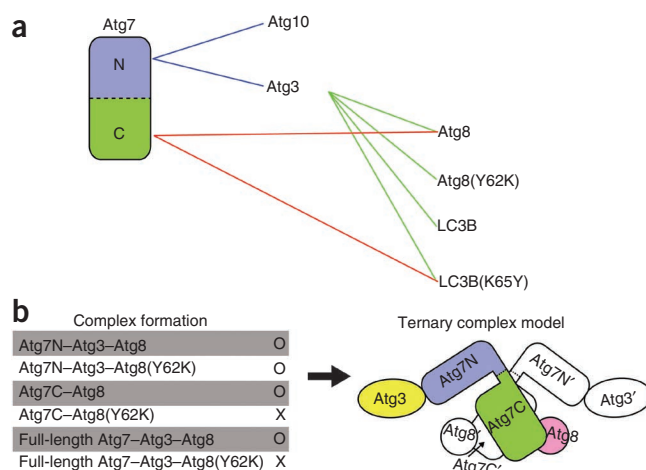## Analysis of the biochemical interaction

Next, we examined the binary interaction between Atg7N and Atg3 in more detail. The structure of Atg3 contains two unique insertions, the HR and FR regions—the latter referred to as the Atg7-binding region[37]. We confirmed that the isolated FR region of Atg3 (Atg3FR) forms a tight complex with Atg7N in solution (**Fig. 5e,f**). Additionally, we performed a competition assay using Atg3 (or Atg3FR) and Atg10 with Atg7N. Atg3 seems to bind with higher affinity to Atg7 than Atg10 does, as it disrupts the preformed Atg7N–Atg10 complex (**Fig. 5c**) to yield the Atg7N–Atg3 complex (**Fig. 5d**).

We also examined Atg7N–Atg3–Atg8 ternary complex formation. The stable ternary complex was formed in solution (**Supplementary Fig. 5c**). As there was no direct interaction between Atg7N and Atg8 (**Supplementary Fig. 5a**), Atg3 probably bridges between Atg7N and Atg8 in the ternary complex. In contrast, Atg7C did not form a ternary complex with Atg8 and Atg3. Instead, only the binary Atg7C–Atg8 complex was formed. The interaction of Atg8 and Atg3 is well established and has been structurally characterized[38–40]. The fact that only the binary complex Atg7C–Atg8 was formed in presence of Atg3 suggests that Atg7C and Atg3 have overlapping binding sites on Atg8 and that the interaction with Atg7C is stronger than that with Atg3. Indeed, comparison of the present Atg7C–Atg8 structure with the

Atg3–Atg8 structure reveals a steric clash that would be expected to preclude ternary complex formation (**Supplementary Fig. 7**).

Full-length Atg7 forms a 2:2 complex with Atg3 (**Supplementary Figs. 6** and **8**), and the complex is very stable in solution, as it did not dissociate in the course of two sequential gel-filtration experiments (**Supplementary Fig. 8b**). Additionally, the ternary complex Atg3–Atg7–Atg8 is stable (**Supplementary Fig. 8**). To better define the interactions in this complex, we assayed its formation using the Y62K mutant Atg8, which is unable to bind Atg7C. With this mutant, only the Atg7–Atg3 binary complex was formed (**Supplementary Fig. 8c**), confirming that Atg3 binds Atg7N and that Atg8 binds Atg7C independently (**Fig. 6a**). **Figure 6** summarizes the binary interactions among Atg7, Atg3, Atg10, Atg8 (wild-type or Y62K mutant) and human LC3B (or K65Y mutant), and the ternary interactions among Atg7, Atg3 and Atg8. Collectively, our biochemical and structural data show that the Atg3–Atg7–Atg8 complex contains six subunits

Figure 6 Interaction map of Atg7 with other autophagic molecules and a model for the Atg3–Atg7–Atg8 ternary complex. (**a**) Binary interaction map based on our gel-filtration results. Lines indicate direct interaction. Blue, red and green lines represent the interaction of Atg7N–E2 enzymes, Atg7C–Atg8s and Atg3–Atg8s, respectively. LC3B is from human; other factors are from yeast. (**b**) Left, summary of gel-filtration results with various mixtures, including full-length Atg7. See **Supplementary Figures 5** and **8** for more details. Right, model of the Atg3–Atg7–Atg8 ternary complex present before thioester bond formation, based on a combination of our gel-filtration results and our structural information. Coloring of Atg3, Atg7N, Atg7C and Atg8 is as in **Figures 1c** and **5b**.

Table 1 Data collection, phasing and refinement statistics

	Atg7N (SeMet)				Atg7C–Atg8 (SeMet)			
Data collection								
Space group	$I4_1$				$P4_32_12$			
Cell dimensions								
a, b, c (Å)	112.8, 112.8, 102.2				71.3, 71.3, 220.9			
	High	*Peak*	*Inflection*	*Remote*	*High*	*Peak*	*Inflection*	*Remote*
Wavelength	1.0	0.9795	0.9798	0.95	1.0	0.9796	0.9799	0.95
Resolution (Å)	2.10 (2.18–2.10)	2.50 (2.59–2.50)	2.50 (2.59–2.50)	2.50 (2.59–2.50)	1.90 (1.97–1.90)	2.50 (2.59–2.50)	2.50 (2.59–2.50)	2.50 (2.59–2.50)
R_{merge}	0.062 (0.705)	0.061 (0.479)	0.060 (0.535)	0.060 (0.571)	0.059 (0.771)	0.079 (0.210)	0.077 (0.275)	0.085 (0.323)
$I / \sigma I$	35.0 (2.9)	37.4 (3.6)	36.3 (3.1)	44.4 (3.4)	30.9 (3.6)	71.9 (16.9)	70.3 (16.1)	68.3 (15.7)
Completeness (%)	99.5 (100)	99.9 (99.9)	99.9 (99.7)	99.9 (99.8)	99.6 (99.3)	100 (100)	100 (100)	100 (100)
Redundancy	7.0	7.0	7.0	7.0	8.1	19.4	19.4	19.4
Refinement								
Resolution (Å)	29.3–2.10				41.6–1.91			
No. reflections	31,750				43,347			
R_{work} / R_{free}	0.209 / 0.236				0.194 / 0.218			
No. atoms								
Protein	2,335				3,504			
Zn^{2+}	–				1			
Water	145				305			
B-factors								
Protein	53.7				32.0 (Atg7C), 54.9 (Atg8)			
Zn^{2+}	–				26.8			
Water	52.3				38.6			
R.m.s. deviations								
Bond lengths (Å)	0.01				0.01			
Bond angles (°)	1.34				1.17			

One selenomethionine crystal for Atg7N and one selenomethionine crystal for the Atg7C–Atg8 complex were used for data collection. Values in parentheses are for highest-resolution shell.

with a 2:2:2 stoichiometry, and that it is organized as an Atg7 dimer with one molecule of Atg3 bound to each of its N-terminal domains and one molecule of Atg8 bound to each of its C-terminal domains (**Fig. 6b**). We propose that this model represents the complex present before thioester bond formation.

DISCUSSION

Here we report structural and biochemical data of the relatively uncharacterized noncanonical E1 enzyme Atg7. One unexpected finding is that the catalytic cysteine residue Cys507 is already located near the C terminus of Atg8 (**Fig. 3c**). This spatial arrangement is similar to that of SUMO E1~SUMO1-AVSN (ref. 18), suggesting that Atg7 adopts a catalytically competent state appropriate for covalent bond formation between Atg7 and Atg8 without a marked conformational rearrangement. This is in stark contrast to the rearrangements associated with canonical E1 enzymes, in which a large conformational change of the catalytic cysteine domain is required for covalent modification[15,18]. ATP binding is the first step in the established reaction mechanism of canonical E1 enzymes, and incoming Ubl is then covalently modified by the adenylation reaction. This adenylation of Ubl molecules is a prerequisite for the subsequent thioester bond formation, and it facilitates movement of a cysteine residue, located more than 30 Å from the active site, toward the active site in the adenylation domain of canonical E1 enzymes. Even in Uba1, whose structure has no ATP ligand as in our Atg7C–Atg8 structure, the distance between the C terminus of ubiquitin and the key cysteine residue is considerable (~35 Å)[16]. Our structure suggests that a comparatively modest local conformational change will be required for formation of a tetrahedral intermediate; the crossover

loop and a short helix containing the key residue Cys507 may need to rearrange in the course of catalysis (**Fig. 3c**)[18].

Previous biochemical and mutational study of Atg8 residues classifies mutants into three groups (classes I, II and III)[41]. Class I mutations such as K48A and L50A substantially reduce autophagic activity[41], and these positions are involved in the interaction with Atg3 (ref. 38). The previous study did not identify Tyr62 of Atg8 as important for the autophagic process, but we found that it is required for Atg7 binding, and mutation of this residue markedly reduced autophagosome formation *in vivo* (**Supplementary Fig. 3b**). When we examined the Atg7–Atg8 interaction surface, interesting features were evident. The mode of binding seems similar to that of the canonical E1 and Ubl interaction, although, unlike in E1, the C-terminal region of Atg7 is crucial in determining specificity, and it is most probably specific only for Atg8, as the C-terminal 17 residues of Atg7 are known to be essential for Atg8 lipidation but not for Atg12 conjugation[29].

The ultimate destination of Atg8, after the intermediate step of binding Atg7, is binding to the E2 enzyme Atg3. The interaction between Atg8 and Atg3 is mediated by the WxxL motif in Atg3. This motif, referred to as the Atg8-family interacting motif (AIM), is found in various Atg8-family proteins, autophagic receptors and even non-autophagic proteins: Atg19, Atg32, Atg3, Atg4B, p62, NBR1, calreticulin, clathrin heavy chain and Nix[39]. The residues that recognize the AIM in Atg8 are Lys46, Lys48, Tyr49, Leu50, Val51, Phe60, Val63 and Ile64 (ref. 38), and hydrophobic Val63 is particularly involved in the Atg7 interaction (**Supplementary Table 2**). Indeed, the WxxL binding region on Atg8 overlaps the region involved in interaction with the C-terminal region of Atg7; hence, Atg8 is unable to simultaneously bind both the E1 enzyme Atg7 and the E2 enzyme Atg3 (**Supplementary Fig. 7**).

When we performed gel-filtration analysis using various combinations of Atg3, Atg7 and Atg8, the ternary complex Atg3–Atg7–Atg8 was obtained (**Fig. 6b**). However, for the final Atg8~Atg3 conjugate product to be formed, the interaction between Atg8 and the C-terminal region of Atg7C found in our structure must be displaced by the WxxL motif in Atg3. As noted above, the crossover loop that facilitates the actual conformational change in Atg7 is located close to the key cysteine residue. Therefore, we speculate that adenylation is used to eject the tightly bound Atg8 molecule from the core of Atg7C. More intriguingly, the transfer of Atg8 from Atg7C to acceptor Atg3 might be mediated by Atg7N from a different subunit, as the potential position of Atg7N in the same polypeptide chain is at the back side of the molecule, and Atg7N from a different subunit would be positioned more closely (**Fig. 3c**). This could account for the fact that noncanonical E1 enzyme Atg7 adopts a homodimeric form (**Fig. 6b**).

Although no structural information on Atg7–Atg12 complex is available, previous *in vivo* and *in vitro* data concerning the Atg7-deletion mutant, which comprises a 17-residue deletion at the C terminus, suggest that the binding mode of Atg12 differs from that of Atg8 (ref. 29) and requires E2 enzyme Atg10 for the conjugation reaction. Furthermore, Atg10 has no detectable WxxL motif, and therefore the interactions involved in Atg12–Atg10 complex formation might differ from those in the Atg8–Atg3 complex. Although we could not provide structural details concerning the E1-E2 interaction, we did examine the affinity of Atg7 for Atg10 and Atg3.

As the FR region in Atg3 has been reported to interact with Atg7 (ref. 37), we generated Atg3FR as well as full-length Atg3 and examined their interactions with Atg7N. Isolated Atg7N formed a complex with Atg3 or Atg3FR, as well as with Atg10 (**Fig. 5c–f**). When we performed competition experiments by gel filtration, Atg3 and Atg3FR each showed higher binding affinity for Atg7N than that of Atg10 for Atg7N (**Fig. 5c–f**).

These data confirm the hierarchical process previously described for autophagosome formation[5,42]. It is known that the majority of Atg8 present in yeast is in an unconjugated form, which might be not be processed by cysteine protease Atg4 under nutrient-rich conditions; when autophagy is induced, Atg8 is converted to the phosphatidyl-ethanolamine (PE)-attached form[43]. Previous *in vivo* systematic and quantitative analysis by fluorescence microscopy has shown that the Atg12 system is located upstream of the Atg8 system and is involved in the organization of pre-autophagosome structures[42]. The reaction product of the Atg12 system, the Atg12~Atg5 conjugate, also enhances formation of the lipid conjugate Atg8~PE *in vitro* in a manner similar to that of ubiquitin E3 ligase[44]. Consistent with a previous report[42], our *in vitro* biochemical data support a postulated hierarchy wherein Atg3 can easily be replaced with bound Atg10 in autophagy (**Fig. 5d**). We also speculate that the binding affinity of Atg8 for Atg7 might be stronger than that of Atg12 for Atg7, as Atg8 is involved in an additional interaction with the C-terminal region of Atg7C (**Fig. 2a**), although this interaction probably occurs only with the mature form of Atg8 containing no C-terminal Arg117 (**Supplementary Fig. 2b**). For a complete understanding of the regulation of both Atg8 and Atg12 systems by Atg7, further biochemical and structural studies on the ternary complex Atg3–Atg7–Atg8 as well as on Atg10–Atg7–Atg12 are required.

METHODS

Methods and any associated references are available in the online version of the paper at http://www.nature.com/nsmb/.

Accession codes. Atomic coordinates and structure factor files have been deposited in the Protein Data Bank with accession codes 3RUI for Atg7C–Atg8 complex and 3RUJ for Atg7N.

1. Nakatogawa, H., Suzuki, K., Kamada, Y. & Ohsumi, Y. Dynamics and diversity in autophagy mechanisms: lessons from yeast. *Nat. Rev. Mol. Cell Biol.* **10**, 458–467 (2009).
2. Klionsky, D.J. & Emr, S.D. Autophagy as a regulated pathway of cellular degradation. *Science* **290**, 1717–1721 (2000).
3. Klionsky, D.J. *et al.* A unified nomenclature for yeast autophagy-related genes. *Dev. Cell* **5**, 539–545 (2003).
4. Noda, N.N., Ohsumi, Y. & Inagaki, F. ATG systems from the protein structural point of view. *Chem. Rev.* **109**, 1587–1598 (2009).
5. Suzuki, K. & Ohsumi, Y. Current knowledge of the pre-autophagosomal structure (PAS). *FEBS Lett.* **584**, 1280–1286 (2010).
6. Shintani, T. & Klionsky, D.J. Autophagy in health and disease: a double-edged sword. *Science* **306**, 990–995 (2004).
7. Rabinowitz, J.D. & White, E. Autophagy and metabolism. *Science* **330**, 1344–1348 (2010).
8. Klionsky, D.J. *et al.* A comprehensive glossary of autophagy-related molecules and processes. *Autophagy* **6**, 438–448 (2010).
9. Levine, B., Mizushima, N. & Virgin, H.W. Autophagy in immunity and inflammation. *Nature* **469**, 323–335 (2011).
10. Mizushima, N. *et al.* A protein conjugation system essential for autophagy. *Nature* **395**, 395–398 (1998).
11. Ichimura, Y. *et al.* A ubiquitin-like system mediates protein lipidation. *Nature* **408**, 488–492 (2000).
12. Varshavsky, A. Regulated protein degradation. *Trends Biochem. Sci.* **30**, 283–286 (2005).
13. Hochstrasser, M. Origin and function of ubiquitin-like proteins. *Nature* **458**, 422–429 (2009).
14. Hershko, A. & Ciechanover, A. The ubiquitin system. *Annu. Rev. Biochem.* **67**, 425–479 (1998).
15. Schulman, B.A. & Harper, J.W. Ubiquitin-like protein activation by E1 enzymes: the apex for downstream signalling pathways. *Nat. Rev. Mol. Cell Biol.* **10**, 319–331 (2009).
16. Lee, I. & Schindelin, H. Structural insights into E1-catalyzed ubiquitin activation and transfer to conjugating enzymes. *Cell* **134**, 268–278 (2008).
17. Huang, D.T. *et al.* Basis for a ubiquitin-like protein thioester switch toggling E1–E2 affinity. *Nature* **445**, 394–398 (2007).
18. Olsen, S.K., Capili, A.D., Lu, X., Tan, D.S. & Lima, C.D. Active site remodelling accompanies thioester bond formation in the SUMO E1. *Nature* **463**, 906–912 (2010).
19. Völler, D. & Schindelin, H. And yet it moves: active site remodeling in the SUMO E1. *Structure* **18**, 419–421 (2010).
20. Bacik, J.P., Walker, J.R., Ali, M., Schimmer, A.D. & Dhe-Paganon, S. Crystal structure of the human ubiquitin-activating enzyme 5 (UBA5) bound to ATP: mechanistic insights into a minimalistic E1 enzyme. *J. Biol. Chem.* **285**, 20273–20280 (2010).
21. Geng, J. & Klionsky, D.J. The Atg8 and Atg12 ubiquitin-like conjugation systems in macroautophagy. *EMBO Rep.* **9**, 859–864 (2008).
22. Zhang, J. & Ney, P.A. Reticulocyte mitophagy: monitoring mitochondrial clearance in a mammalian model. *Autophagy* **6**, 405–408 (2010).
23. Komatsu, M. *et al.* Impairment of starvation-induced and constitutive autophagy in Atg7-deficient mice. *J. Cell Biol.* **169**, 425–434 (2005).
24. Mortensen, M. *et al.* The autophagy protein Atg7 is essential for hematopoietic stem cell maintenance. *J. Exp. Med.* **208**, 455–467 (2011).
25. Lenz, H.D., Vierstra, R.D., Nurnberger, T. & Gust, A.A. ATG7 contributes to plant basal immunity towards fungal infection. *Plant Signal. Behav.* **6**, 1040–1042 (2011).

26. Komatsu, M. *et al.* The C-terminal region of an Apg7p/Cvt2p is required for homodimerization and is essential for its E1 activity and E1–E2 complex formation. *J. Biol. Chem.* **276**, 9846–9854 (2001).

27. Noda, T., Fujita, N. & Yoshimori, T. The Ubi brothers reunited. *Autophagy* **4**, 540–541 (2008).

28. Holm, L. & Rosenstrom, P. Dali server: conservation mapping in 3D. *Nucleic Acids Res.* **38**, W545–W549 (2010).

29. Yamazaki-Sato, H., Tanida, I., Ueno, T. & Kominami, E. The carboxyl terminal 17 amino acids within Apg7 are essential for Apg8 lipidation, but not for Apg12 conjugation. *FEBS Lett.* **551**, 71–77 (2003).

30. Lake, M.W., Wuebbens, M.M., Rajagopalan, K.V. & Schindelin, H. Mechanism of ubiquitin activation revealed by the structure of a bacterial MoeB-MoaD complex. *Nature* **414**, 325–329 (2001).

31. Lehmann, C., Begley, T.P. & Ealick, S.E. Structure of the *Escherichia coli* ThiS-ThiF complex, a key component of the sulfur transfer system in thiamin biosynthesis. *Biochemistry* **45**, 11–19 (2006).

32. Lois, L.M. & Lima, C.D. Structures of the SUMO E1 provide mechanistic insights into SUMO activation and E2 recruitment to E1. *EMBO J.* **24**, 439–451 (2005).

33. Harding, M.M. Small revisions to predicted distances around metal sites in proteins. *Acta Crystallogr. D Biol. Crystallogr.* **62**, 678–682 (2006).

34. Reynolds, C., Damerell, D. & Jones, S. ProtorP: a protein-protein interaction analysis server. *Bioinformatics* **25**, 413–414 (2009).

35. Hurley, J.H., Lee, S. & Prag, G. Ubiquitin-binding domains. *Biochem. J.* **399**, 361–372 (2006).

36. Sato, Y. *et al.* Structural basis for specific cleavage of Lys 63-linked polyubiquitin chains. *Nature* **455**, 358–362 (2008).

37. Yamada, Y. *et al.* The crystal structure of Atg3, an autophagy-related ubiquitin carrier protein (E2) enzyme that mediates Atg8 lipidation. *J. Biol. Chem.* **282**, 8036–8043 (2007).

38. Yamaguchi, M. *et al.* Autophagy-related protein 8 (Atg8) family interacting motif in Atg3 mediates the Atg3-Atg8 interaction and is crucial for the cytoplasm-to-vacuole targeting pathway. *J. Biol. Chem.* **285**, 29599–29607 (2010).

39. Noda, N.N., Ohsumi, Y. & Inagaki, F. Atg8-family interacting motif crucial for selective autophagy. *FEBS Lett.* **584**, 1379–1385 (2010).

40. Ichimura, Y. *et al.* Structural basis for sorting mechanism of p62 in selective autophagy. *J. Biol. Chem.* **283**, 22847–22857 (2008).

41. Nakatogawa, H., Ichimura, Y. & Ohsumi, Y. Atg8, a ubiquitin-like protein required for autophagosome formation, mediates membrane tethering and hemifusion. *Cell* **130**, 165–178 (2007).

42. Suzuki, K., Kubota, Y., Sekito, T. & Ohsumi, Y. Hierarchy of Atg proteins in pre-autophagosomal structure organization. *Genes Cells* **12**, 209–218 (2007).

43. Huang, W.P., Scott, S.V., Kim, J. & Klionsky, D.J. The itinerary of a vesicle component, Aut7p/Cvt5p, terminates in the yeast vacuole via the autophagy/Cvt pathways. *J. Biol. Chem.* **275**, 5845–5851 (2000).

44. Hanada, T. *et al.* The Atg12-Atg5 conjugate has a novel E3-like activity for protein lipidation in autophagy. *J. Biol. Chem.* **282**, 37298–37302 (2007).

ONLINE METHODS

Protein expression and purification. For the structural investigation of Atg7 from *S. cerevisiae*, two separate domains were cloned comprising the N- and C-terminal regions, residues 1–294 and 293–630, respectively. The amplified PCR products, treated with restriction enzymes BamHI and EcoRI, were inserted into a modified pET vector for the construction of glutathione S-transferase (GST)–tagged protein. The resultant plasmids were transformed into Rosetta (DE3) cells. Expression of proteins was induced by the addition of 0.5 mM IPTG (and 0.1 mM ZnCl$_2$ in the case of Atg7C) at 18 °C for 24 h. Cells were harvested by centrifugation and resuspended in PBS containing 1 mM tris-(2-carboxyethyl)phosphine (TCEP). After sonication, the cell lysate was loaded onto a glutathione–Sepharose 4B affinity column and then eluted with 10 mM glutathione. The GST tag was cleaved using TEV protease, and the resultant proteins (starting with Gly-Ser residues after the first methionine) were further purified by ion-exchange column using 5 ml Q FF or S FF (GE Healthcare). Finally, proteins were loaded onto a 16/60 Superdex75 gel-filtration column (GE Healthcare) pre-equilibrated with 50 mM Tris-HCl (pH 8.0), 200 mM NaCl and 2 mM TCEP (for Atg7C; conditions were the same for Atg7N except that 50 mM HEPES (pH 7.0) was used). Selenomethionine-substituted Atg7N and Atg7C were expressed in *Escherichia coli* B834(DE3) cells with defined medium and purified in a similar manner to that described for the wild-type proteins.

All other proteins, including full-length Atg7, Atg3, Atg10, Atg8, mutants Atg3FR (residues 84–161), Atg7CΔ9, Atg7CΔ15 and Atg7CΔ27, and human LC3B, were also cloned into the modified GST-tagged vector and purified in a similar manner to that described above for Atg7C or Atg7N. Mutant proteins (mutations Y62K, Y62A, K66E, K66A, and Y62A K66A in Atg8; C507S, E612A, E612Q and E612R in Atg7C; and K65Y in human LC3B) were generated using the QuikChange mutagenesis kit (Stratagene), and mutant samples were prepared in the same way as wild-type proteins.

Crystallization and data collection. Purified Atg7C (C507S mutant) and Atg8 were mixed in a molar ratio of 1:2 at 4 °C for 30 min and reloaded onto a gel-filtration column for purification of the complex. Samples were concentrated to ~10–14 mg ml^{-1} and crystallized by hanging-drop vapor diffusion at 22 °C, after mixing of an equal volume of reservoir solution containing 0.1 M HEPES (pH 7.5), ~7–10% (w/v) PEG 3,350 and 20 mM proline. Crystals of the complex were obtained within 1–2 d and transferred sequentially to mother liquor solutions with 5%, 10% and 20% (v/v) glycerol added for dehydration. Atg7N was concentrated to 16 mg ml^{-1}, and crystals were also obtained by hanging-drop vapor diffusion at 22 °C with a reservoir solution containing 0.1 M HEPES (pH 8.0), 1.5 M Li$_2$SO$_4$ and 0.1 M spermidine tetrahydrochloride. Crystals were flash-frozen with reservoir solution containing 20% (v/v) glycerol before being flash-frozen in a nitrogen stream at 100 K.

MAD data for Atg7C–Atg8 were collected at the 4A beamline of Pohang Accelerator Laboratory, Pohang, South Korea, and high-resolution data were collected at the NW12 beamline of Photon Factory, Tsukuba, Japan. MAD and high-resolution data for Atg7N were collected at the NE3-A beamline of Photon Factory. Diffraction data were indexed, integrated and scaled using the HKL2000 software package[45]. Statistics for the collected data are listed in **Table 1**.

Structure determination and refinement. All of the eight possible selenium sites in the asymmetric unit of Atg7C–Atg8 crystal, and two of three possible sites in Atg7N, were located using three-wavelength MAD data sets. Initial phases were calculated, and initial models for Atg7C–Atg8 and Atg7N were built automatically using the PHENIX package program[46] with up to 90% of Atg7C–Atg8 and only 20% of the Atg7N polypeptide chain. Models were rebuilt manually using COOT and O[47,48]. Refinement was also carried out using the PHENIX package program, and model geometry was assessed and secondary structure elements assigned with MolProbity[49] and STRIDE[50]. For structure comparison, DALI (http://ekhidna.biocenter.helsinki.fi/dali_server/) was used[28], and all structural images were drawn using PyMOL (http://www.pymol.org/).

Biochemical assays. Atg7C~Atg8 thioester bond formation was assayed in a reaction mixture containing 3.7 μM Atg7C, 12.7 μM Atg8 (C-terminal Gly116 exposed), 10 mM MgCl$_2$, 5 mM ATP, 50 mM Tris-HCl (pH 8.0), 200 mM NaCl and 1.5 mM TCEP at 22 °C. Assays with mutants or LC3B were performed under similar conditions. Incubated mixture was denatured by nonreducing sample buffer, subjected to SDS-PAGE and then visualized by Coomassie blue staining. The band corresponding to the Atg7C~Atg8 covalent complex was also confirmed by mass-spectrometric analysis.

A competitive binding assay using Atg10 and Atg3 with the Atg7N domain was performed sequentially. First, Atg7N–Atg10 complex was further purified using gel filtration. Atg7N–Atg3FR was also prepared by the same methods. Similar molar ratios of E2s were then mixed with complexed proteins (Atg3 with Atg7N–Atg10 or Atg10 with Atg7N–Atg3FR), and samples were loaded onto a Superdex 75 10/300 GL gel-filtration column. We generated Atg3–Atg7–Atg8 complex by initially generating Atg7–Atg3, then adding Atg8. This complex was loaded onto a Superdex 200 10/300 GL column. All gel-filtration experiments were performed with buffer containing 50 mM Tris-HCl (pH 8.0) or 50 mM HEPES (pH 7.0), 150 mM NaCl and 1.5 mM TCEP. Gel-filtration data were analyzed and graphed using the UNICORN 5.11 program (GE Healthcare).

Size-exclusion chromatography with multi-angle light scattering. Size-exclusion chromatography with multi-angle light scattering (SEC-MALS) experiments were performed using a FPLC system (GE Healthcare) connected to a Wyatt MiniDAWN TREOS MALS instrument and a Wyatt Optilab rEX differential refractometer. A Superdex 200 10/300 GL (GE Healthcare) gel-filtration column pre-equilibrated with 20 mM HEPES (pH 7.5), 150 mM NaCl and 2 mM TCEP was normalized using BSA protein. Complexed or individual uncomplexed protein, prepared by the methods described above, was injected (~1–3 mg ml^{-1}, 0.5 ml) at a flow rate of 0.5 ml min^{-1}. Data were evaluated using the Zimm model for static light-scattering data fitting and graphed using EASI Graph with a UV peak in the ASTRA V software (Wyatt).

45. Otwinowski, Z. & Minor, W. Processing of X-ray diffraction data collected in oscillation mode. *Methods Enzymol.* **276**, 307–326 (1997).
46. Adams, P.D. *et al.* PHENIX: a comprehensive Python-based system for macromolecular structure solution. *Acta Crystallogr. D Biol. Crystallogr.* **66**, 213–221 (2010).
47. Emsley, P. & Cowtan, K. Coot: model-building tools for molecular graphics. *Acta Crystallogr. D Biol. Crystallogr.* **60**, 2126–2132 (2004).
48. Jones, T.A., Zou, J.-Y., Cowan, S.W. & Kjeldgaard, M. Improved methods for binding protein models in electron density maps and the location of errors in these models. *Acta Crystallogr. A* **47**, 110–119 (1991).
49. Chen, V.B. *et al.* MolProbity: all-atom structure validation for macromolecular crystallography. *Acta Crystallogr. D Biol. Crystallogr.* **66**, 12–21 (2010).
50. Heinig, M. & Frishman, D. STRIDE: a web server for secondary structure assignment from known atomic coordinates of proteins. *Nucleic Acids Res.* **32**, W500–W502 (2004).